Efficient Preamble Detection and Time-of-Arrival Estimation for Single-Tone Frequency Hopping Random Access in NB-IoT

Houcine Chougrani, Steven Kisseleff, *Member, IEEE*, and Symeon Chatzinotas, *Senior Member, IEEE*

***Abstract*—The narrowband Internet-of-Things (NB-IoT) standard is a new cellular wireless technology, which has been introduced by the 3rd generation partnership project (3GPP) with the goal to connect massive low-cost, low-complexity and long-life IoT devices with extended coverage. In order to improve power efficiency, 3GPP proposed a new random access (RA) waveform for NB-IoT based on a *single-tone frequency-hopping* scheme. RA handles the first connection between user equipments (UEs) and the base station (BS). Through this, UEs can be identified and synchronized with the BS. In this context, receiver methods for the detection of the new waveform should satisfy the requirements on the successful user detection as well as the timing synchronization accuracy. This is not a trivial task, especially in the presence of radio impairments like carrier frequency offset (CFO) which constitutes one of the main radio impairments besides the noise. In order to tackle this problem, we propose a new receiver method for NB-IoT physical RA channel (NPRACH). The method is designed to eliminate perfectly the CFO without any additional computational complexity and supports all NPRACH preamble formats. The associated performance has been evaluated under 3GPP conditions. We observe a very high performance compared both to 3GPP requirements and to the existing state-of-the-art methods in terms of detection accuracy and complexity.**

***Index Terms*—3rd generation partnership project (3GPP), carrier frequency offset (CFO), frequency hopping, narrowband Internet of Things (NB-IoT), NB-IoT physical random access channel (NPRACH), random access (RA), Time of Arrival (ToA).**

I. Introduction

THE MAIN goal of the upcoming Internet of Things (IoT) is to interconnect various kinds of devices in order to make existing systems more intelligent, responsive, and robust. It is envisioned that IoT will have a considerable economic and societal impact. Ericsson [1] reported that the number of IoT connected devices expected to exceed 4.1 billion by 2024. This results in a variety of use cases with different requirements and methodologies leading to a necessity of tailored communication technology. Correspondingly, many technologies appeared in both licensed and unlicensed markets, see [2]–[4], and among them the norrowband-IoT (NB-IoT), which is a recent cellular technology standardized by 3rd generation partnership project (3GPP) in 2016 [4], [5]. It aims at providing connectivity to billions of IoT devices, supporting low device cost, long battery lifetime, and wide coverage. NB-IoT inherits from the existing long term evolution (LTE) technology. The radio access is based on orthogonal frequency-division multiple access (OFDMA) for downlink and single-carrier frequency-division multiple access (SC-FDMA) for uplink with 180-kHz system bandwidth. The reason for that was to allow a better co-existance with Legacy LTE, the reuse of existing infrastructures, and reduction of time to market. However, some changes have been introduced in NB-IoT compared to LTE to ensure the aforementioned objectives. In [6] and [7], these changes are summarized and discussed.

One of the differences between NB-IoT and LTE is in the so-called random access (RA) procedure. A new waveform is designed for the RA in NB-IoT compared to the traditional signaling using Zadoff–Chu sequences employed in LTE RA [8]. This change has been introduced in order to reduce the peak-to-average power ratio (PAPR), thus improving the battery lifetime of the device and the coverage in the context of IoT network. It is worth noting that high PAPR requires a large backoff for the power amplifier (PA) in general, which leads to a low efficiency of the PA and correspondingly a low battery lifetime. Moreover, high PA backoff reduces the radiated signal power and reduces the coverage. In contrast, the new NB-IoT physical RA channel (NPRACH) waveform has very good PAPR properties. The NPRACH waveform is specified as *single-tone frequency hopping* preamble [8]. On the other hand, the new waveform is still compatible with the LTE SC-FDMA and OFDMA schemes, and it is typically treated as an OFDM signal with one subcarrier [8], [9].

Similarly to the RA in LTE, the RA in NB-IoT manages the uplink synchronization and the requests of scheduling of data transmissions. In this context, the uplink synchronization means that the base station (BS) has to detect (and identify) all active user equipments (UEs) in the coverage area of the BS and estimate their round-trip delays (RTDs). Through this, the delay between each UE and the BS is acquired, which represents a common timing reference. The acquired delay allows

Manuscript received September 2, 2020; revised October 8, 2020; accepted November 12, 2020. Date of publication November 18, 2020; date of current version April 23, 2021. This work was supported in part by the Luxembourg National Research Fund (FNR) in the Framework of the FNR-IPBG Project "INSTRUCT: Integrated Satellite-Terrestrial Systems for Ubiquitous Beyond 5G Communication," and in part by the FNR-CORE "5G-Sky: Interconnecting the Sky in 5G and Beyond—A Joint Communication and Control Approach." *(Corresponding author: Houcine Chougrani.)*

The authors are with the Interdisciplinary Centre for Security, Reliability and Trust, University of Luxembourg, 1855 Luxembourg City, Luxembourg (e-mail: houcine.chougrani@uni.lu; steven.kisseleff@uni.lu; symeon.chatzinotas@uni.lu).

Digital Object Identifier 10.1109/JIOT.2020.3039004

the BS to perform timing advance needed to keep the orthogonality among multiple UEs, which is typically required in SC-FDMA systems. The estimation of RTD refers to a Time-of-Arrival (ToA) estimation, whereas the user detection refers to NPRACH preamble detection. It is worth noting that this operation is essential for a successful system operation. In fact, RA is the first phase of system operation and covers the first messages from each UE to the BS. Hence, a wrong detection and/or an erroneous ToA estimation would lead to increased latency and performance degradation for the system. In practice, when a user is not correctly detected, another round of RA procedure is started, which implies an increased power consumption as well as additional delays in data packet transmission. The latter is also responsible for a decrease of the overall system throughput. On the other hand, when the detection is correct and only the ToA is inaccurate, the timing synchronization might be lost, which may lead to an increased packet error rate. Furthermore, the performance degradation depends on the ToA error: large errors can completely damage the data exchange. In order to avoid this, 3GPP standard [10] provides the requirements for the maximum rate of wrong detections and for the maximum ToA error in NPRACH.

One of the challenges in any communication system is the presence of a random carrier frequency offset (CFO). It can be produced by imperfect local oscillators (LOs), Doppler shift, or downlink frequency synchronization errors in case of 3GPP-based communication.

For the ToA estimation in SC-FDMA system, the CFO contributes to the phase rotation of the received complex signal in a similar way as the timing offset. Correspondingly, it is difficult to separate the influence of CFO and ToA on the received signal, such that the accuracy of the ToA estimation is typically very low in presence of CFO. In this context, there are few works that addressed the NPRACH reception design. The first work in this domain [9] has been filed [11]. The proposed technique is based on a 2-D fast Fourier transform (FFT) for a joint estimation of CFO and ToA. Then the preamble detection is performed comparing the metric used for the ToA estimate with a predefined threshold. The main drawback of this method is its computational complexity, which is extremely high due to the 2-D-FFT, which makes this method impractical.

In [12], a low-complexity NPRACH receiver design has been proposed. It decouples the detection problem from the estimation problem. The detection is based on energy detection scheme and the collected signal energy is compared with the optimal threshold derived by the authors. The estimation is based on the CFO estimation and subsequent compensation. Then, the ToA is estimated from the phase of the received signal. In [12], the performance of the detection part was provided with the assumed absent CFO. This is not a realistic assumption for practical scenarios, where CFO is present and impacts the signal-to-noise ratio (SNR). Moreover, the method has a processing delay that increases with the number of preamble repetitions leading to a less efficient real-time system as pointed out in [13]. Another relevant work that has been recently submitted for a publication is [13]. The author provides a detailed and useful mathematical model for the NPRACH signals. However, the proposed method supports only small ToA values, i.e., ToA $\leq$ 66.7 us (which is defined as format 0 in the 3GPP Standard). In this method, at first the CFO is estimated (with capability limitation, i.e., the maximum tolerated CFO is $\leq$ 357 Hz) from the received signal and then compensated. After that, the ToA estimation is performed using 1-D FFT, which leads to lower computational complexity compared to [9] and [11]. The detection part is done by comparing the metric based on ToA estimate with a predefined threshold, which has been obtained experimentally. Unfortunately, this method has some weaknesses with respect to both performance and complexity. First, it is limited to NPRACH format 0 (ToA $\leq$ 66.7 us), such that users with larger ToA (e.g., NPRACH format 1) cannot be detected. Second, the estimation and the compensation of the CFO leads to a degradation of the ToA estimation performance in case of inaccurate CFO estimation and compensation. Furthermore, both CFO estimation and compensation contribute to the receiver complexity.

Based on this state-of-the-art analysis, it becomes apparent that all the existing techniques follow the classical way of dealing with a synchronization problem (i.e., either CFO estimation and compensation before timing estimation or joint frequency and timing estimation). Though this, the system performance deteriorates in terms of energy efficiency, flexibility, and/or reliability. In order to mitigate the aforementioned weaknesses, we propose in this article a novel efficient NPRACH reception technique, which is resistant to the presence of frequency errors. The main contributions of this article are summarized as follows.

1) Design of an efficient NPRACH reception method that allows to detect the NPRACH preamble and to estimate the ToA. The technique can address all NPRACH formats, and it is designed in a way that the CFO present in the received signal is perfectly eliminated. Hence, no estimation and compensation of the CFO are required. This allows not only to reduce the computational complexity, but also to avoid ToA errors coming from an imperfect CFO estimation and compensation. An extension of the method is also provided as a generalization of the proposed method to further improve the performance.
2) Performance evaluation and comparison with 3GPP requirements as well as with the most relevant state-of-the-art works [13], [14]. A complexity analysis is also provided. The obtained results demonstrate a large margin compared to 3GPP requirements and the superiority of the proposed method compared to the previous works. Furthermore, these interesting results are obtained with less complexity compared to the complexity of the existing methods. The comparison shows 50% of complexity reduction compared to [13]. This high performance can be supposedly exploited in order to reduce the overhead (e.g., the NPRACH preamble length) leading to increased spectral and energy efficiencies, which are very crucial in the context of IoT systems.

The remainder of this article is organized as follows. The NPRACH scheme as well as the system model are described in Section II. In Section III, a novel method of preamble detection

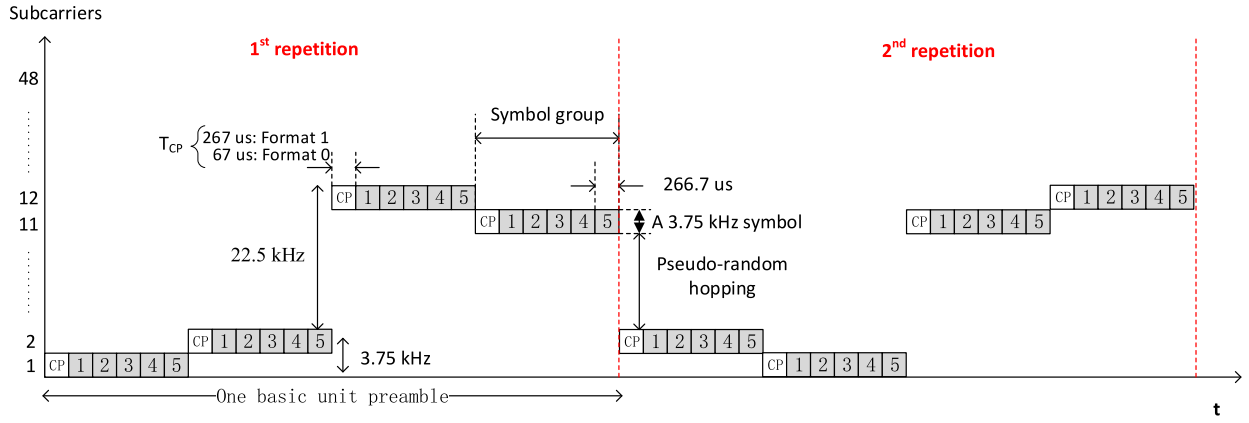

Fig. 1. NPRACH preamble frame structure.

and ToA estimation is proposed. The numerical results, comparison with 3GPP requirements and state-of-the-art works, as well as complexity analysis, are provided and discussed in Section IV. Finally, Section V concludes this article.

II. System Model

For the clarity of exposition, we employ the same notation and same variable definitions as provided in the 3GPP standard [8], [15] and previous works [13], [14].

The RA preamble in NB-IoT known as NPRACH preamble was originally proposed by [16]–[19] and then adopted by 3GPP and integrated in NB-IoT Release 13 [4]. It is based on single-tone, frequency-hopping scheme as illustrated in Fig. 1. The preamble consists of four symbol groups (SGs). Each SG is composed of five identical symbols with a cyclic prefix (CP) and occupies one tone of 3.75 kHz in frequency domain. The CP length is designed according to the targeted cell size. It can be either 66.67 us for preamble format 0 (i.e., corresponding to a cell radius of 10 km), or 266.67 us for preamble format 1 (i.e., corresponding to a cell radius of 40 km). Traditionally, the preamble is considered as a single-tone OFDM symbol with 3.75-kHz subcarrier spacing. This single-tone OFDM symbol signal, however, hops between frequency tones from SG to SG following a predefined pattern to enable a satisfactory ToA estimation. In the 3GPP standard, four SGs are treated as the basic unit of the preamble. This basic unit can be repeated up to $2^j, j = \{0, 1, \ldots, 7\}$ times for coverage extension. Accordingly, the length L of a preamble equals 4×2^j SGs [9]. The hopping pattern is fixed within the basic unit of four SGs. Between the SGs {0, 1} and {2, 3} the hopping distance equals one subcarrier spacing. Between the SGs {3, 4} the distance equals six subcarrier spacings. However, when repetitions are configured, the hopping between the basic units is no longer fixed, but follows a pseudo-random selection procedure defined in [8].

In NB-IoT system, each UE determines the time and frequency resources to transmit the NPRACH preamble based on the system information block broadcasted by the BS during the downlink. According to the 3GPP standard [8], [15], the possible resource configurations are as follows.

1) $N_{\text{period}}^{\text{NPRACH}}$ is the period of time within which NPRACH can be transmitted. Possible values are: $N_{\text{period}}^{\text{NPRACH}} \in \{40, 80, 160, 240, 320, 640, 1280, 2560\}$ ms.
2) $N_{\text{rep}}^{\text{NPRACH}}$ denotes the number of NPRACH preamble repetitions per attempt. Possible values are: $N_{\text{rep}}^{\text{NPRACH}} \in \{1, 2, 4, 8, 16, 32, 64, 128\}$.
3) $N_{scoffset}^{\text{NPRACH}}$ corresponds to the index of the first subcarrier allocated to NPRACH within 180-kHz bandwidth. Possible values are: $N_{scoffset}^{\text{NPRACH}} \in \{0, 12, 24, 36, 2, 18, 34\}$.
4) N_{SC}^{NPRACH} corresponds to the number of subcarriers allocated to NPRACH. Possible values are: $N_{SC}^{\text{NPRACH}} \in \{12, 24, 36, 48\}$.
5) $N_{\text{start}}^{\text{NPRACH}}$ corresponds to NPRACH transmission starting time. Possible values are: $N_{\text{start}}^{\text{NPRACH}} \in \{8, 16, 32, 64, 128, 256, 512, 1024\}$ ms. NPRACH transmission can start only $N_{\text{start}}^{\text{NPRACH}}$ subframes after the first subframe in radio frames fulfilling $\text{mod}\,(n_f, (N_{\text{period}}^{\text{NPRACH}}/10)) = 0$, where n_f is the system frame number.

In practice, each UE selects randomly the starting subcarrier n_{init} from $\{0, \ldots, N_{SC}^{\text{NPRACH}} - 1\}$ for the first SG. The next 3 subcarrier locations (corresponding to the next 3 SGs) are determined by a specific algorithm (based on modulo sum) which depends only on the location of the first subcarrier. For the subcarrier selection of the first SG of the next repetition, a pseudo-random hopping, which utilizes a cell-ID as its initial seed, is applied. The subcarrier selection for the subsequent SGs depends only on the outcome of pseudo-random hopping [8]. Note that with a single-tone and subcarrier spacing of 3.75 kHz, a cell can configure 12, 24, 36, or 48 starting subcarriers for the NPRACH within the 180-kHz NB-IoT system bandwidth. This means that up to 48 orthogonal preambles are available to transmit an NPRACH. In short, each UE selects randomly one preamble among the 48 available and transmitted to the BS in the NPRACH resource. Fig. 2 shows an example of 12 multiplexed UEs in an NPRACH resource. We note that if the same preamble is selected by two or more UEs, a collision is declared.

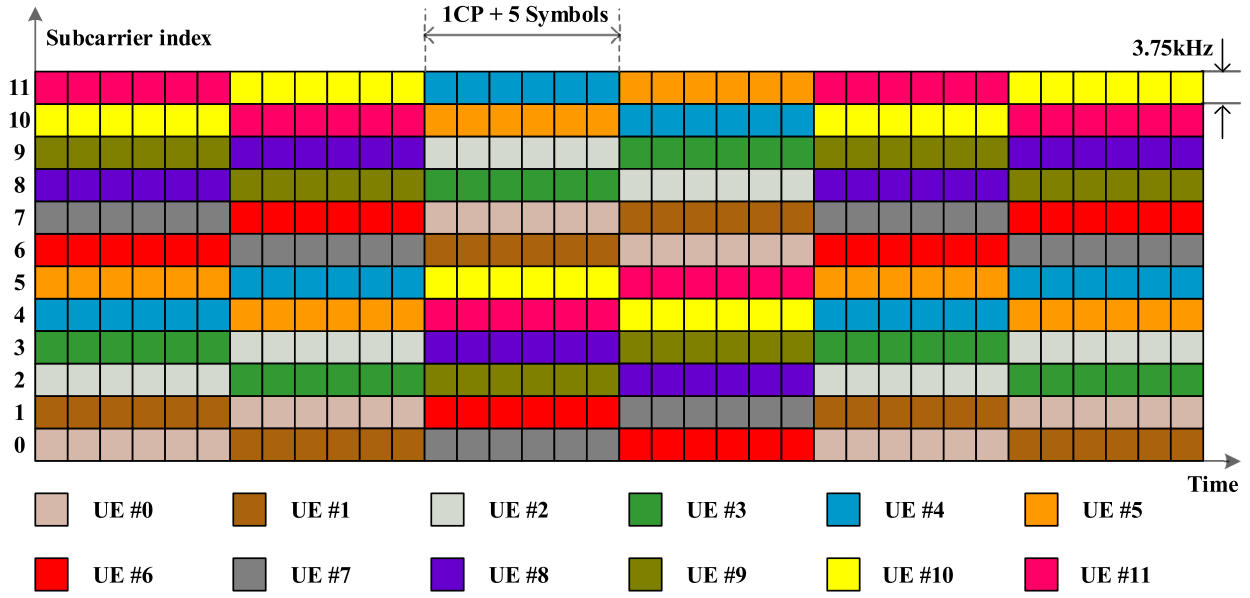

Fig. 2. Example of 12 UEs NPRACH multiplexing.

At the receiver side, the BS tries to identify all 48 frequency hopping patterns (i.e., preamble signatures). The ones successfully identified represent the active UEs. In this configuration, the kth UE is identified by its n_{init} in the range $\{0, \ldots, N_{SC}^{\text{NPRACH}} - 1\}$ that allows to construct the pattern as explained above.

Based on [9] and [13], the transmitted baseband signal for the NPRACH preamble can be written as follows:

$$s_{m,i}[n] = \sum_{k} S_{m,i}[k] e^{j2\pi \frac{k}{N} n} \tag{1}$$

where $s_{m,i}[n]$ is the nth sample of the time domain waveform of ith symbol in mth SG and $S_{m,i}[k]$ denotes the ith symbol on the kth subcarrier during the mth SG. Furthermore, $n = [N_{m,i} - N_{CP}, \ldots, N_{m,i}+N-1]$, $i = [0, \ldots, 4]$, where $N_{m,i} = mN_g + iN$, $N_g = N_{cp} + 5N$ is the size of one SG, N_{cp} is the size of CP, N is the size of a symbol.

Before providing the model for the received signal, it is worth noting that the NB-IoT channel varies extremely slowly in time. This comes from the fact that NB-IoT is not intended to support high mobility of the devices [20]. Accordingly, the channel is assumed to be invariant in time within at least 3 SGs and flat within 45-kHz frequency band (i.e., 12 subcarrirs). This means that the channel response does not change at least during three SGs within 45-kHz bandwidth. The validity of these assumptions is discussed in the Appendix. Based on [9] and [13], the nth sample of ith symbol in mth SG of the received signal $y_{m,i}[n]$ can be written as

$$\begin{aligned} y_{m,i}[n] &= h_m e^{j2\pi f_{\text{off}}(n-D)} s_{m,i}[n-D] + w_{m,i}[n] \\ &= h_m e^{j2\pi f_{\text{off}}(n-D)} \sum_{k} S_{m,i}[k] e^{j2\pi \frac{k}{N}(n-D)} \\ &\quad + w_{m,i}[n] \end{aligned} \tag{2}$$

where f_{off} is the CFO normalized by the sampling frequency, D is the RTD normalized by the symbol duration; h_m is the channel coefficient at mth SG. In addition, $w_{m,i}[n]$ is complex additive white Gaussian noise (AWGN) with zero mean and variance N_0. By removing the CP (i.e., N_{cp} samples) and performing FFT, we obtain

$$\begin{aligned} Y_{m,i}[l] &= \sum_{n=N_{m,i}}^{N_{m,i}+N-1} y_{m,i}[n] e^{-j2\pi ln/N} \\ &= \sum_{n=N_{m,i}}^{N_{m,i}+N-1} h_m e^{j2\pi f_{\text{off}}(n-D)} \\ &\quad \times \sum_{k} S_{m,i}[k] e^{j2\pi \frac{k}{N}(n-D)} e^{-j2\pi ln/N} \\ &\quad + W_{m,i}[l] \end{aligned} \tag{3}$$

where $W_{m,i}[l]$ denotes the frequency response of the noise signal. By exchanging the variables $n' = n - N_{m,i}$, (3) can be expressed as

$$\begin{aligned} Y_{m,i}[l] &= h_m e^{j2\pi f_{\text{off}}(N_{m,i}-D)} \sum_{k} S_{m,i}[k] e^{-j2\pi \frac{k}{N} D} \\ &\quad \times \sum_{n'=0}^{N-1} e^{j2\pi f_{\text{off}} n'} e^{j2\pi \frac{(k-l)}{N}(n'-N_{m,i})} + W_{m,i}[l] \\ &= h_m e^{j2\pi f_{\text{off}}(N_{m,i}-D)} S_{m,i}[l] e^{-j2\pi l \frac{D}{N}} \sum_{n'=0}^{N-1} e^{j2\pi f_{\text{off}} n'} \\ &\quad + h_m e^{j2\pi f_{\text{off}}(N_{m,i}-D)} \sum_{k \neq l} S_{m,i}[k] e^{-j2\pi \frac{k}{N} D} \\ &\quad \times \sum_{n'=0}^{N-1} e^{j2\pi f_{\text{off}} n'} e^{j2\pi \frac{(k-l)}{N}(n'-N_{m,i})} + W_{m,i}[l] \\ &= Y_{m,i}^{sig}[l] + Y_{m,i}^{ICI}[l] + W_{m,i}[l]. \end{aligned} \tag{4}$$

The above equation shows that the received signal consists of a signal term ($Y_{m,i}^{sig}$), intercarrier interference (ICI) term ($Y_{m,i}^{ICI}$) and a noise term ($W_{m,i}$).

As specified in [8], the symbols $S_{m,i}[n_{SC}^{RA}(m)]$ are all identically equal to 1 for any m, i and the same (mth) SG. Here, $n_{SC}^{RA}(m)$ is the subcarrier occupied by mth SG. Assuming that ICI is negligible, when $l = n_{SC}^{RA}(m)$ holds, the received signal becomes

$$Y_{m,i} = h_m e^{j2\pi f_{\text{off}}(mN_g+iN-D)} \times e^{-j2\pi n_{SC}^{RA}(m)\frac{D}{N}} \frac{1-e^{j2\pi f_{\text{off}}N}}{1-e^{j2\pi f_{\text{off}}}} + W_{m,i}. \quad (5)$$

By combining the signals within the same mth SG, we get SG-Sum (SG-S)

$$Y_m = \sum_{i=0}^{4} Y_{m,i} = h_m e^{j2\pi f_{\text{off}}(mN_g-D)} \times e^{-j2\pi n_{SC}^{RA}(m)\frac{D}{N}} \frac{1-e^{j2\pi f_{\text{off}}5N}}{1-e^{j2\pi f_{\text{off}}}} + W_m \quad (6)$$

where W_m is the noise term. This result will be used in the next section for the design of the optimal method for preamble detection and ToA estimation.

III. Proposed Method for Preamble Detection and ToA Estimation

In this section, the proposed method is described, which aims at detecting the NPRACH preamble and estimating the ToA in presence of CFO. Unlike classical synchronization schemes that either estimate jointly the timing offset with CFO or estimate and compensate the CFO in the received signal before estimating the timing, the proposed method eliminates perfectly the CFO and estimates directly the timing offset (i.e., ToA). For the proposed method and its extended version, we employ different sets of the combinations of SGs. Accordingly, the core of the proposed method only employs a small number of combination. We refer to this method as "Differential processing with minimum combinations." The extended version of the method is based on a more advanced processing, which includes additional combinations of SGs. Thus, more information can be extracted from the received signal, which helps to improve the estimation accuracy. We refer to this extended version as "Differential processing with extended combinations." Both versions are explained in the following.

A. Differential Processing With Minimum Combinations

1) Elimination of the CFO and Signal Preparation: At first, we perform a differential processing of the neighboring SGs by multiplying the mth SG-S with the complex conjugated $(m+1)$th SG-S

$$Z_{m,1} = Y_m Y_{m+1}^* = Q|h_m|^2 e^{-j2\pi f_{\text{off}}N_g} e^{j2\pi\Delta(m)\frac{D}{N}} + \widetilde{W}_{m,1}, \quad (7)$$

$$Q \triangleq \left| \frac{1-e^{j2\pi f_{\text{off}}5N}}{1-e^{j2\pi f_{\text{off}}}} \right|^2 \quad (8)$$

$$\widetilde{W}_{m,1} \triangleq Y_m^{sig} W_{m+1}^* + Y_{m+1}^{sig*} W_m + W_m W_{m+1}^* \quad (9)$$

where $\Delta(m) = n_{SC}^{RA}(m+1) - n_{SC}^{RA}(m)$ is the hopping step between the mth and $(m+1)$th SGs and $\widetilde{W}_{m,1}$ is the noise term of $Z_{m,1}$. This operation is performed for all SGs, including the pseudo-random hopping between the repetitions (if configured).

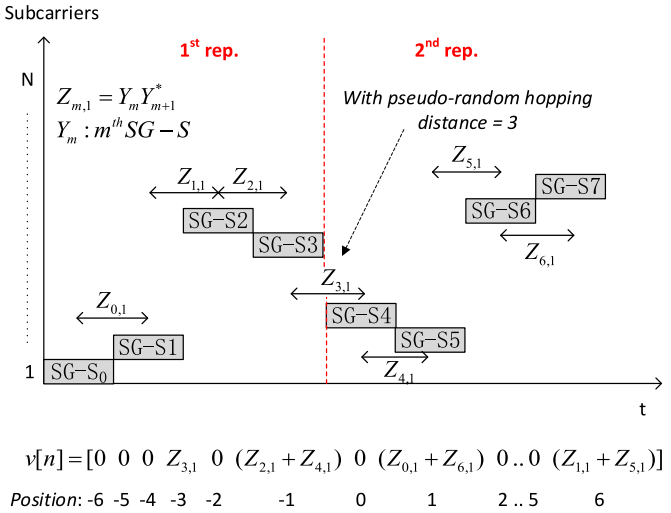

Fig. 3. Differential processing with minimum combinations.

Second, we construct a vector $v[n]$ of length 13 in such a way, that the $(7+\Delta(m))$th element of $v[n]$ is equal to $Z_{m,1}$. The numbers 13 and 7 are selected according to the maximum subcarrier spacing between two consecutive SGs, which is assumed to be 6. Apparently, in order to account for both positive and negative values of $\Delta(m)$ in the range between -6 and 6, vector $v[n]$ needs to have 13 elements, where the 7th element corresponds to $\Delta(m) = 0$. Note, that there might be multiple $Z_{m,1}$ with equal value of $\Delta(m)$, i.e., $\Delta(m_1) = \Delta(m_2)$ with $m_1 \neq m_2$, their values are summed up before being inserted in $v[n]$. To clarify this, Fig. 3 illustrates an example of NPRACH preamble with two repetitions (i.e., two basic preamble units). As an example, we assume in the figure that the hopping steps of the preamble are $\Delta(m) = [1, 6, -1, -3, -1, 6, 1]$. Accordingly, we obtain a vector $v[n]$ with 13 elements at respective positions between -6 and 6, i.e., $v[n] = [0, 0, 0, Z_{3,1}, 0, (Z_{2,1}+Z_{4,1}), 0, (Z_{0,1}+Z_{6,1}), 0, 0, 0, 0, (Z_{1,1}+Z_{5,1})]$.

Note that the CFO is still present in the vector $v[n]$, since it affects the phase of the symbols $Z_{m,1}$ that constitute it. Rather than estimating the CFO and compensating it in the signal as performed in [13], we ensure here that the CFO factor is common for all $Z_{m,1}$ symbols. This is valid, if we consider a differential processing only for neighboring SGs (see (7)). Accordingly, and since the phase rotation of noise does not affect its probability distribution (due to the circular symmetry of the noise), we can pull the common factor $e^{-j2\pi f_{\text{off}}N_g}$ out of vector $v[n]$ to obtain

$$v[n] = e^{-j2\pi f_{\text{off}}N_g} v'[n] \quad (10)$$

such that $v'[n]$ is independent from f_{off}. Obviously, $v'[n]$ only depends on ToA,[1] which has a similar impact on $v'[n]$ like the classical frequency offset on the received signals in

[1] Vector $v'[n]$ also contains the noise terms according to the derivations of $Z_{m,1}$.

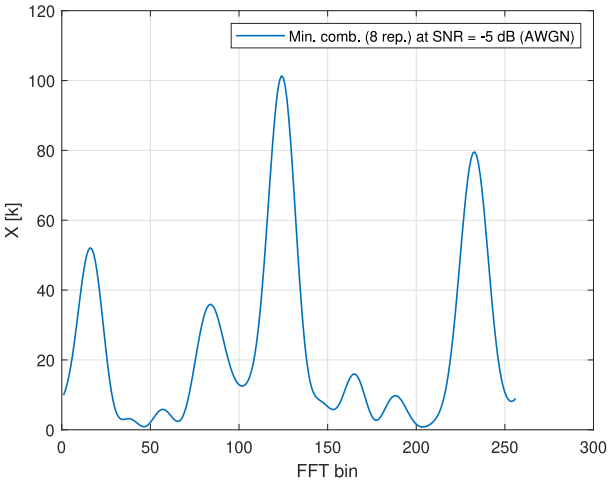

Fig. 4. Example of post-FFT spectrum of vector v.

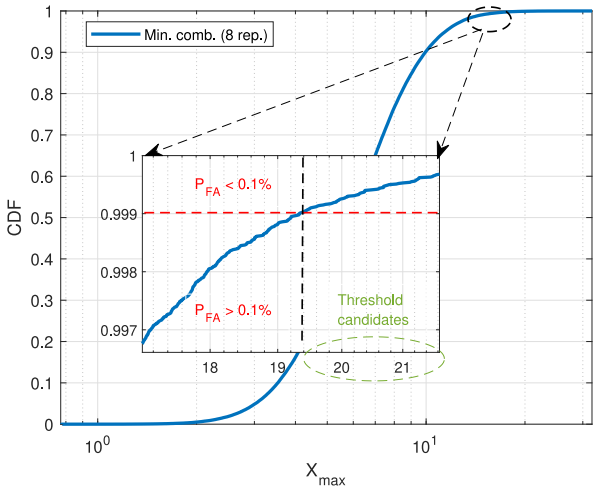

Fig. 5. Empirical CDF of $X_{\max}$ in absence of signal (i.e., only noise).

traditional wireless communications. Hence, in order to estimate ToA, we perform the well-known Rife&Boorstyn (R&B) method (see [21]), which resembles an approximation of the maximum-likelihood frequency offset estimation. Accordingly, the next step is to perform an 1-D-FFT on $v[n]$, and take the absolute maximum of the results. This can be written as

$$U[k] = \sum_{n=0}^{N_{\text{FFT}}-1} v[n] e^{-j2\pi k \frac{n}{N_{\text{FFT}}}} \tag{11}$$

where N_{FFT} is the number of FFT points. Since the FFT is a linear operation, using (11), we can express

$$U[k] = e^{-j2\pi f_{\text{off}} N_g} U'[k], \tag{12}$$

$$U'[k] = \sum_{n=0}^{N_{\text{FFT}}-1} v'[n] e^{-j2\pi k \frac{n}{N_{\text{FFT}}}} \tag{13}$$

where $U'[k]$ is independent from f_{off}. Hence, by taking the absolute of $U[k]$ we eliminate the impact of CFO given by $e^{-j2\pi f_{\text{off}} N_g}$ term, since it affects only the phase of $U[k]$, not its magnitude.

Combining noncoherently over the two receive antennas, we obtain

$$X[k] = \sum_{N_{rx}} |U[k]|^2. \tag{14}$$

Fig. 4 shows an example of the 256-FFT spectrum of the vector v at SNR = -5 dB under AWGN channel. The next step is to determine $X_{\max} = \max_k\{X[k]\}$ and $k_{\max} \in [0, N_{\text{FFT}}]$, for which $X_{\max} = X[k_{\max}]$. Similarly to the frequency estimation using the R&B method, the resolution of the ToA estimation (i.e., $\Delta\hat{D}$) depends on the N_{FFT}, since it can be expressed as $\Delta\hat{D} = (1/\Delta f/N_{\text{FFT}})$ where Δf is the subcarrier spacing of NPRACH (i.e., 3.75 kHz). Of course, by increasing the number of FFT points a much better resolution and estimation accuracy can be achieved. At this stage, we first make a decision on the presence of the preamble, then we deduce the ToA value.

2) Preamble Detection: To declare the presence of the preamble, we compare the metric $X_{\max}$ to a predefined threshold τ. This threshold is currently set through simulations. In practice the threshold can be determined experimentally. In order to determine the threshold, the metric $X_{\max}$ is first calculated via multiple attempts to receive a preamble in absence of the useful signal, i.e., only noise is present. Then the cumulative distribution function (CDF) of the $X_{\max}$ values is obtained. The threshold τ is set equal to the $X_{\max}$ value, which pertains to the probability of 99.9% (corresponding to the false alarm rate of 0.1%) as shown in Fig. 5. Taking into account all possible preamble lengths, every preamble repetition has its own threshold τ calculated as above and stored in a look-up table. The detection of the preamble ($P_{\text{detection}}$) is decided online (both signal and noise are present)

$$P_{\text{detection}}(n_{\text{init}}) = \begin{cases} 1, & \text{if } X_{\max} \geq \tau \\ 0, & \text{otherwise} \end{cases}. \tag{15}$$

If the noise level varies considerably during the system operation, the predefined threshold τ may need to be calculated taking into account the noise power. In this case, the metric $X_{\max}$ obtained in absence of the useful signal is normalized by the noise power. Then, the threshold is determined in a similar way by selecting the value, which pertains to the probability of 99.9%. In this configuration, the decision for the preamble detection is done with the help of an estimate of the noise variance, which can be obtained from the collected statistics across SGs, repetitions and antennas. For this, the metric $X_{\max}$ is first normalized with the estimated noise variance. The result is compared with the threshold τ. Note that the threshold becomes independent from the noise and preamble parameters due to the normalization. However, this strategy requires an accurate estimation of the noise variance during the NPRACH reception as described in [13], which can be challenging in practice.

3) ToA Calculation: If the presence of the preamble is declared, the ToA is calculated as follows[2]:

$$\hat{D}'(n_{\text{init}}) = \frac{k_{\max}}{N_{\text{FFT}}\Delta f}. \tag{16}$$

In order to further increase the accuracy of the estimation, we perform a well-known and frequently used quadratic interpolation around the maximum $X_{\max}$ [22], and compute

[2]Note, that $k_{\max}$ can obtain values between 0 and $N_{\text{FFT}}-1$, where $k_{\max} = 0$ implies $D = 0$.

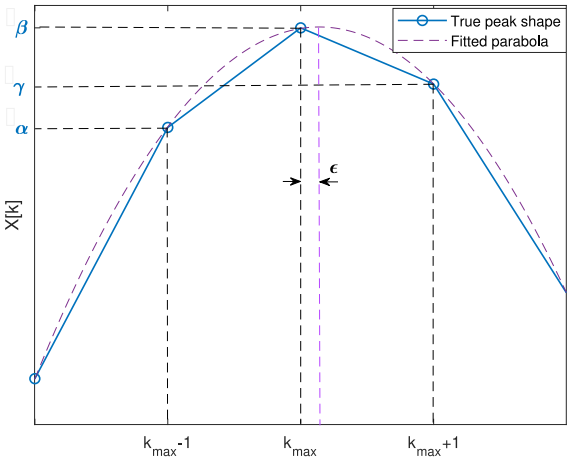

Fig. 6. Quadratic interpolation of spectral peak [22].

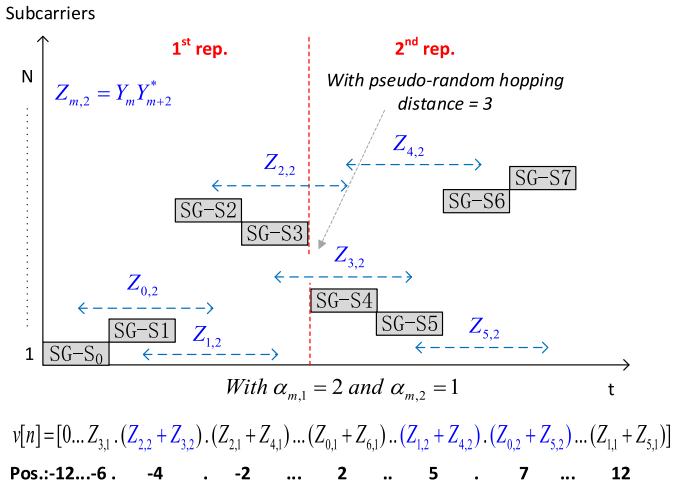

Fig. 7. Differential processing with extended combinations ($c_{\max} = 2$, i.e., $c = 1$ and $c = 2$).

the location of the maximum of the interpolation function. Accordingly, the final ToA estimate is given by

$$\hat{D}(n_{\text{init}}) = \hat{D}'(n_{\text{init}}) + \epsilon \frac{1/\Delta f}{N_{\text{FFT}}} \tag{17}$$

where $\epsilon = (1/2)[(\gamma - \alpha/2\beta - \alpha - \gamma)]$, and α, β, and γ are the indices corresponding to $X[k_{\max}-1]$, $X[k_{\max}]$, and $X[k_{\max}+1]$, respectively, as shown in Fig. 6.

It is worth noting here, that for NPRACH format 0, where the RTD is known to not exceed the CP length of 66.67 us, the maximum is determined only within the CP-window length plus the maximum tolerated error, which equals ±3.646 us for NPRACH according to [10]. This reduces the probability of spurious peaks outside of the coverage area that may outperform the correct peak in some cases. Correspondingly, the method can be made more robust by reducing the search range.

B. Differential Processing With Extended Combinations

The method proposed above can be extended in order to further improve the accuracy of ToA estimation. For this, we consider more SG combinations within the preamble basic unit (i.e., 4 SGs) and over repetition (if configured). In particular, we focus on combinations of SGs with indices that differ by at most $c_{\max}$, where $c_{\max}$ is a strictly positive integer. If $c_{\max} = 1$ holds, only the neighbouring SGs are combined according to the method described in Section III-A and we end up with the minimum number of SG combinations. If $c_{\max} \geq 2$ holds, there are more possibilities for the SG combinations and we refer to these combinations as extended. In this case all combinations $c \leq c_{\max}$ are considered. The main difference between the method outlined above and its extended version is the way of how these extended combinations are incorporated in the calculation. For the mth combination with the difference c between the SG indices, we multiply the mth SG-S with the conjugate of $(m + c)$th SG-S

$$Z_{m,c} = Y_m Y^*_{m+c} = Q|h_m|^2 e^{-j2\pi(cf_{\text{off}})N_g} e^{j2\pi\Delta_c(m)\frac{D}{N}} + \widetilde{W}_{m,c}, \tag{18}$$

$$\widetilde{W}_{m,c} \triangleq Y^{sig}_m W^*_{m+c} + Y^{sig*}_{m+c} W_m + W_m W^*_{m+c} \tag{19}$$

where $\Delta_c(m) = n^{RA}_{SC}(m + c) - n^{RA}_{SC}(m)$ is the hopping step between the mth and $(m+c)$th SGs, and $\widetilde{W}_{m,c}$ is the noise term of $Z_{m,c}$. Next, we determine the minimum common multiple M of all $c \leq c_{\max}$. Then, we multiply the phase of each $Z_{m,c}$ by the factor $\alpha_{m,c} = (M/c)$ in order to obtain the multiple of the CFO as a common factor for all $Z_{m,c}$. Thus, we obtain

$$Z'_{m,c} = Q|h_m|^2 e^{-j2\pi(Mf_{\text{off}})N_g} e^{j2\pi\alpha_{m,c}\Delta_c(m)\frac{D}{N}} + \widetilde{W}'_{m,c}, \tag{20}$$

$$\widetilde{W}'_{m,c} = \left|\widetilde{W}_{m,c}\right| e^{j\alpha_{m,c}\Phi_{\widetilde{W}_{m,c}}}. \tag{21}$$

We can note that $e^{-j2\pi(Mf_{\text{off}})N_g}$ (the term containing CFO) is independent from c and hence it is a common factor for all $Z'_{m,c}$ symbols. At this stage, the vector $v[n]$ is constructed with length of $2L_{m,c} + 1$, and filled with $Z'_{m,c}$ symbols for all $c \leq c_{\max}$ at $(L_{m,c} + \alpha_{m,c}\Delta_c(m) + 1)$th positions, where $L_{m,c} \triangleq \max_{\forall m,c} |\alpha_{m,c}\Delta_c(m)|$.

Fig. 7 shows an example of extended combinations with $c_{\max} = 2$, i.e., $c = 1$, $c = 2$ and $M = 2$. The original hopping pattern of the example is the same as the previous one (i.e., example depicted in Fig. 3), which is $\Delta_1(m) = [1, 6, -1, -3, -1, 6, 1]$. For $c = 1$ (black $Z_{m,1}$ symbols in Fig. 7), we multiply the phase of $Z_{m,1}$ by $\alpha_{m,1} = M/1 = 2$. The hopping of these symbols becomes $\alpha_{m,1} \times \Delta(m) = [2, 12, -2, -6, -2, 12, 2]$. This is why the black symbols are placed at positions $-6, -2, 2$ and 12 in vector $v[n]$. As a reminder, all symbols with the same position within $v[n]$ are summed up. For $c = 2$ (i.e., blue $Z_{m,2}$ symbols in Fig. 7), $\alpha_{m,1} = M/2 = 1$ and $\Delta_2(m) = [7, 5, -4, 5, 7]$. The $Z_{m,2}$ is placed in $v[n]$ at the positions $\Delta_2(m)$, and no phase multiplication is required in this case.

The next steps of the method are the same as with the minimum combinations. The FFT is performed on $v[n]$, then the $[X_{\max}, k_{\max}]$ quantities are determined. If the preamble detection is declared, the ToA is deduced as described above.

TABLE I
SIMULATION PARAMETERS

Parameter	Value
No. of active UEs	1
Preamble format	0 and 1
No. of repetitions	8 and 32
Cell ID (hopp. seed)	Randomly chosen from [0, 503]
Sampling rate	1.92 MHz
Subcarrier spacing	3.75 kHz
NPRACH band	12 subcarriers (45 kHz)
Antenna config. [10]	1 Tx, 2 Rx
Timing offset	Randomly selected within: [0, 66.67] us or [0, 259] us
Propagation channels	AWGN, EPA1, ETU1
Frequency offset	0 Hz (AWGN), 200 Hz (EPA1, ETU1)
FFT size (i.e. N_{FFT})	256 points

IV. SIMULATION RESULTS AND DISCUSSION

In this section, we provide numerical results for the performance evaluation of the proposed NPRACH reception method. When referring to the basic version of the method, we denote it a proposed method with minimum combinations in order to distinguish from the extended version with extended combinations. When referring to extended version of the proposed method, we focus on extended combinations described by $c_{\max} = 2$ according to Section III-B. The method has been implemented in MATLAB and simulated under the 3GPP test conditions. Table I summarizes the link-level simulation parameters. Both preamble formats 0 and 1 are simulated. Accordingly, the timing offset is selected randomly in the interval $[0, 66.67]$ us for preamble format 0, and $[0, 259]$ us for preamble format 1. The number of repetitions is set to 8 or 32. We chose a timing offset limit of 259 us rather than 266.67 us for Format 1 in order to keep a safety interval of $\pm 2 \cdot 3.646$ us that helps to avoid the phase ambiguity. AWGN, extended pedestrian A model with 1 Hz Doppler (EPA1) and extended typical urban model (ETU) with 1-Hz Doppler (ETU1) radio channel models are considered. It is worth noting that 3GPP considers only AWGN (without CFO) and EPA1 (with 200 Hz CFO) channels for NPRACH test requirements, i.e., not ETU1. Nevertheless, we include the ETU1 channel for completeness, since 3GPP may add this channel to the NPRACH requirements in future releases. The number of FFT points used in the method is set to 256 points for a fair comparison with the work in [13].

A. 3GPP Requirements and Performance Metrics

Regarding the performance metric, the 3GPP requirement is expressed in [10] in terms of the minimum SNR, for which the probability of preamble detection is greater than or equal to 99% (i.e., missed detection rate below 1%), and false alarm probability being less than or equal to 0.1%.

According to [10], the probability of detection is defined as the conditional probability of correct detection of the preamble when the signal is present. There are several error cases:

1) detection of a wrong preamble (different than sent);
2) no detection of any preamble;
3) correct preamble detection but with the wrong timing (ToA) estimation.

This latter occurs, if the estimation error of the timing is larger than 3.646 us.

The false alarm probability is defined as the conditional total probability of erroneous detection of the preamble when input only contains the noise, i.e., in absence of the useful signal.

To summarize, the performance metric is the minimum required SNR, for which the preamble is correctly detected and the ToA error is below 3.646 us in 99% of cases while the false alarm probability is below 0.1%.

B. Obtained Results

The obtained results are depicted in Figs. 8–10 for AWGN, EPA1 and ETU1 radio channels, respectively.

For AWGN (see Fig. 8) with 8 repetitions, the missed detection target of 10^{-2} (which corresponds to detection probability $\geq$ 99%) is reached at SNR of -7.68 dB and -9.41 dB for the minimum and extended combinations, respectively. A gain of 1.73 dB is observed with extended combinations compared to the minimum combinations. In case of 32 repetition, the missed detection target is reached at -12.7 dB for minimum combinations and at -13.7 dB for extended combinations, respectively, which leads to 1 dB gain between the two cases. We observe only a slight deviation of these SNR values for preamble format 1 compared to format 0, such that the proposed method can be applied without change for both formats.

For EPA1 (see Fig. 9), the missed detection target is reached at SNR of -2.6 dB and -3.8 dB for minimum and extended combinations, respectively, in case of 8 repetitions. For 32 repetitions, the target performance is reached at -7.5 dB and -8.2 dB for minimum and extended combinations, respectively. Under ETU1 (see Fig. 10) channel, the observed SNR for the missed detection target is -1.4 dB and -3.8 dB for minimum and extended combinations in case of 8 repetitions. For 32 repetitions, the SNR at the missed detection target for minimum and extended combinations is about -6.33 dB and 8.10 respectively. Like the AWGN observation, these SNR levels are almost the same for both preamble formats 0 and 1. In addition, we observe that the false alarm is less than 0.1% in all considered scenarios.

C. Comparison and Discussion

To evaluate these results, a comparison of the proposed work with the 3GPP requirements [10] and with the most representative state-of-the-art works [13], [14] is provided in the following. It is worth noting here that the relevant performance analysis for the algorithm proposed in [11] has been provided in [14].

The numerical results, which are relevant for the comparison, are provided in Figs. 8–10, and summarized in Table II. Note that the results for the ETU1 channel are provided only for the sake of completeness, since no requirements have been imposed by 3GPP for this type of channel yet. First of all, the obtained performance meets the 3GPP requirements [10] for both preamble formats and with both minimum and extended combinations. Under the AWGN channel and for all numbers of repetitions (i.e., $N_{\text{rep}}^{\text{NPRACH}}$ = 8 or 32) a margin of $\approx$

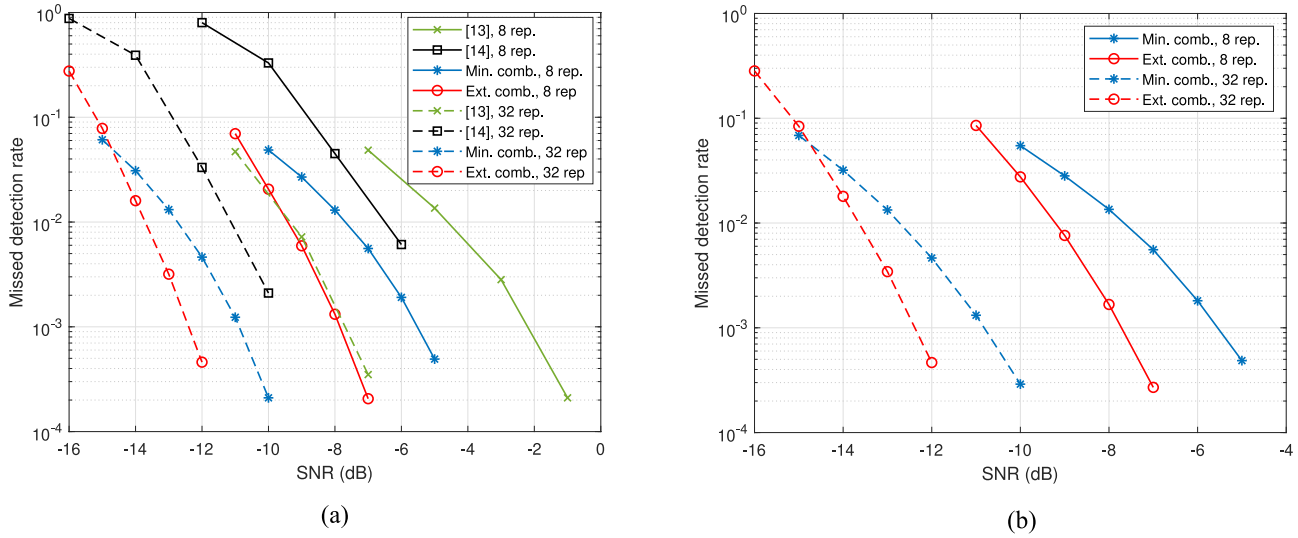

Fig. 8. NPRACH simulation results under AWGN channel for differential processing with minimum (i.e., $c_{\max} = 1$) and extended (i.e., $c_{\max} = 2$) combinations. (a) AWGN channel (0 Hz) for Format 0. (b) AWGN channel (0 Hz) for Format 1.

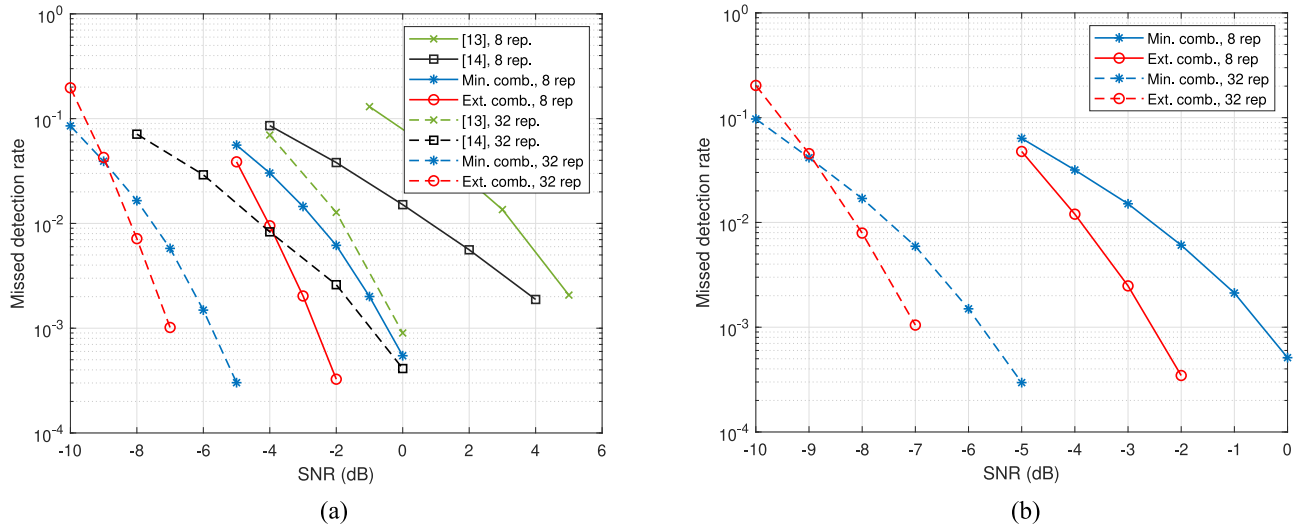

Fig. 9. NPRACH simulation results under EPA1 channel for differential processing with minimum (i.e., $c_{\max} = 1$) and extended combinations (i.e., $c_{\max} = 2$). (a) EPA1 channel (200 Hz) for format 0. (b) EPA1 channel (200 Hz) for format 1.

5.5 dB (in case of minimum combinations) and $\approx$ 7 dB (in case of extended combination) is observed compared to 3GPP requirements. Under EPA1 channel, even larger margins are observed. Interestingly, $\approx$ 8.6 and 10 dB margins are obtained in case of minimum and extended combinations, respectively. These large margins demonstrate a very high accuracy of our proposed method.

Regarding the works in [13] and [14], the performance is compared only for preamble format 0 in AWGN and EPA1 channels, since the method proposed in [13] does not support format 1 and the method in [14] provides only performance analysis for format 0. For ETU1, only preamble format 0 with 8 repetitions is compared, since [14] provides the results only for this configuration. The proposed method clearly outperforms the methods in [13] and [14] in all considered cases.

Under AWGN channel and for any number of repetitions, performance margins of at least 3.1 and 1.1 dB are observed (at missed detection target of 10^{-2}) compared to [13] and [14], respectively, with just the minimum combinations. With extended combinations, these margins increase to at least 4.5 dB and 2.5 dB compared to [13] and [14], respectively. One can see (see Fig. 8(a)) that the performance of [13] with 32 repetitions is equivalent to the performance of the proposed method with only eight repetitions in case of extended combination, such that the preamble detection can be done four times faster.

Interestingly, under EPA1 and ETU1 channels, the margins are even larger. The proposed method can even outperform the other methods with lower repetitions (see Fig. 9(a)). Regarding the work in [13], and in case of 8 repetitions, margins of 6.2 and 7.65 dB are observed (at missed detection target of 10^{-2}) with minimum and extended combinations, respectively, while in case of 32 repetitions, these margins are $\approx$ 5.77 and 6.43 dB. Compared to [14], the observed margins under EPA1 channel are 3.26 and 4.7 dB with minimum and extended

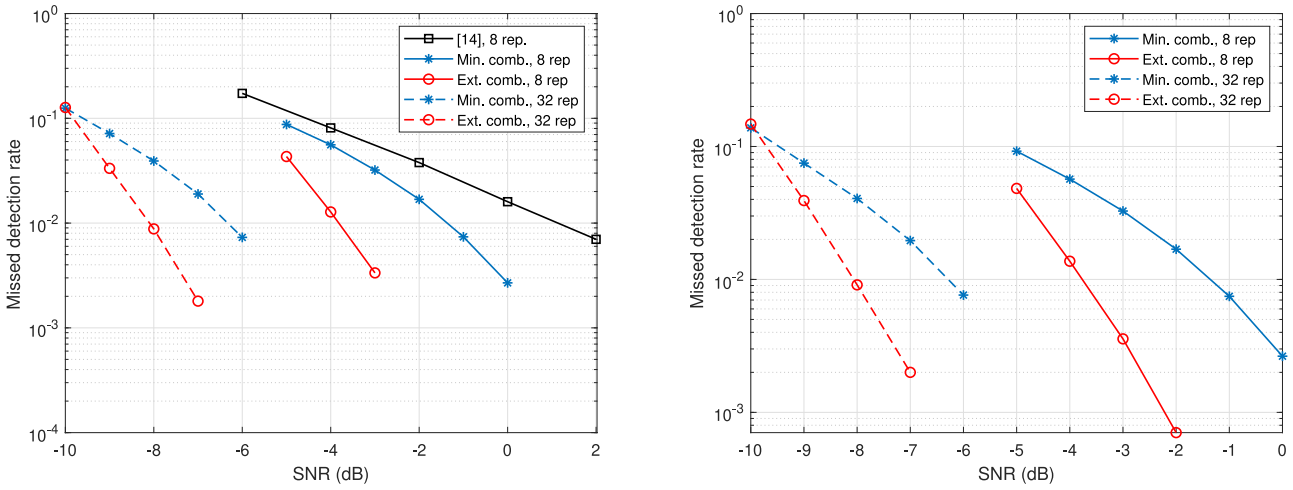

Fig. 10. NPRACH simulation results under ETU1 channel for differential processing with minimum (i.e., $c_{\max} = 1$) and extended combinations (i.e., $c_{\max} = 2$). (a) ETU1 channel (200 Hz) for format 0. (b) ETU1 channel (200 Hz) for format 1.

TABLE II
PERFORMANCE SUMMARY AND COMPARISON

Preamble Format	$N_{\text{rep}}^{\text{NPRACH}}$	Channel	SNR [dB]				
			3GPP Req. [10]	[13]	[14]	Proposed Min. combin.	Proposed Ext. combin.
0	8	AWGN (0 Hz)	-2.1	-4.5	-6.5	-7.68	-9.41
		EPA1 Low (200 Hz)	6.1	3.65	0.7	-2.56	-4
		ETU1 Low (200 Hz)	-	-	1.2	-1.4	-3.8
	32	AWGN (0 Hz)	-6.8	-9.23	-11.2	-12.7	-13.7
		EPA1 Low (200 Hz)	0.5	-1.75	-4.3	-7.52	-8.18
		ETU1 Low (200 Hz)	-	-	-	-6.33	-8.10
1	8	AWGN (0 Hz)	-2.1	-	-	-7.68	-9.22
		EPA1 Low (200 Hz)	6.1	-	-	-2.54	-3.85
		ETU1 Low (200 Hz)	-	-	-	-1.36	-3.76
	32	AWGN (0 Hz)	-6.8	-	-	-12.72	-13.64
		EPA1 Low (200 Hz)	0.5	-	-	-7.5	-8.13
		ETU1 Low (200 Hz)	-	-	-	-6.28	-8

combinations, respectively, if the number of repetitions is 8. For 32 repetitions, the margin remains approximately the same with minimum combinations (i.e., 3.2 dB), whereas with extended combinations the margin decreases to 3.88 dB. Under ETU1 channel, the observed margins are 2.6 and 5 dB with minimum and extended combinations, respectively.

In the following, we provide a brief explanation for such a substantial performance improvement using our method by analyzing the potential weaknesses of the state-of-the-art methods. The method in [14] is based on 2-D-FFT [11], as mentioned earlier. In general, when the CFO is absent, the performance of this method is theoretically close to our method with minimum combinations. This is why only 1 dB gain is observed in case of minimum combination under AWGN channel compared to [14]. This remaining 1 dB gain can be explained by the fact that in our method, the pseudo-random hopping is included in the pre-FFT vector $v[n]$ (see Section III-A) in contrast to [9]. By adding a pseudo-random hopping (which is not fixed) in $v[n]$ allows to increase diversity within the vector leading to higher post-FFT peak and hence a better performance. For the extended combination, the additional gain is the result of adding more symbols to $v[n]$ vector due to higher number of combinations compared to the minimum combinations. In a realistic scenario with a nonvanishing CFO (i.e., EPA1, ETU1), the method in [14] is sensitive to the CFO. A joint estimation of multiple parameters (CFO and ToA in case of [14]) is typically less accurate under the same conditions than the estimation of just one parameter (ToA in case of the proposed method), if all other parameters are either known or perfectly eliminated. This is why at least 2.6 dB gain is observed in ETU1 channel using the proposed method.

A very high performance gain obtained with the proposed method compared to the method in [13] is explained by the sensitivity of the latter to the CFO. The estimation and compensation of the CFO not only leads to additional complexity, but also to a degradation of the ToA estimation performance, since imperfect CFO estimation and compensation leads to residual CFO, which dramatically affects the accuracy of ToA estimation.

In the light of these results, one can notice that the performance of the proposed technique is substantially higher, especially in the realistic scenario with nonvanishing CFO. This high performance can be exploited to reduce the number

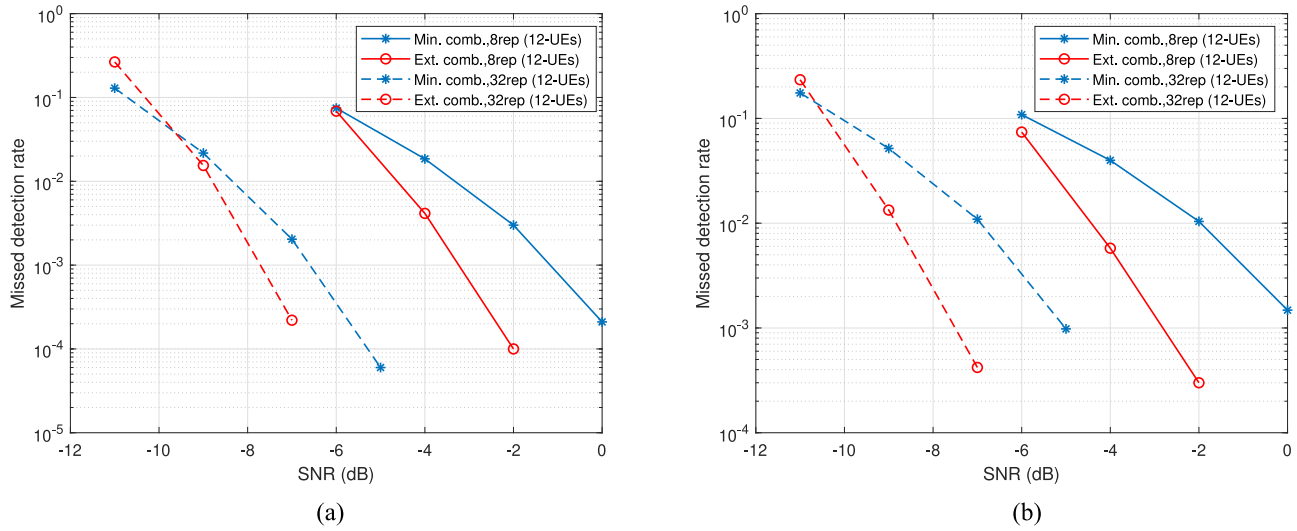

Fig. 11. NPRACH simulation results with 12-active UEs under EPA1 and ETU1 channels. (a) EPA1 channel. (b) ETU1 channel.

of repetitions within the NPRACH preamble while satisfying the 3GPP requirements. Correspondingly, a successful synchronization can be achieved faster, leading to overhead reduction, and thus to an increase of the energy and spectral efficiency desired in the context of IoT system.

The proposed algorithm can work with any frequency hopping pattern under the assumption that this pattern is known to the receiver. However, the maximum delay offset (e.g., RTD) that can be estimated corresponds to the reciprocal minimum hopping distance. Furthermore, the hopping pattern impacts the spectrum of the vector v (after the FFT processing), such that the detection and the estimation performance depends on the pattern. Hence, the design of the optimal pattern should be addressed in future works by taking into account the peculiarities of signal detection associated with the proposed algorithm.

D. Performance in Practical System

To evaluate the performance of the proposed method in a practical system, simulations have been conducted with 12 active UEs under realistic scenarios with nonvanishing CFO. Accordingly, the CFO is no longer fixed (e.g., 200 Hz) as before but randomly selected (with uniform distribution) in the interval $\pm$ 200 Hz. Furthermore, we assume realistic signal propagation models, i.e., EPA1 and ETU1. Note that the previous simulations with a single UE and with fixed CFO 200 Hz represent a pessimistic case, since in a real scenario the CFO is not fixed but uniformly distributed in the range between -200 Hz and 200 Hz. Since the results are very similar for format 0 and 1, we provide the results only for format 1 due to space limitations. Except for the parameters mentioned above, all other simulation parameters remain unchanged, see Table I. The obtained results are depicted in Fig. 11. Similarly to the previous simulations, the performance of the extended combinations is better than with the minimum combinations. For EPA1 channel 8 repetitions (see Fig. 11(a)), the SNR corresponding to the missed detection rate below 1% is -3.3 dB and -4.6 dB for minimum and extended combinations, respectively. With 32 repetitions, these values are -8.3 dB and -8.8 dB. For ETU1 channel (see Fig. 11(b)), the observed SNRs at the missed detection target are -1.9 dB and -4.4 dB with 8 repetitions for minimum and extended combination, respectively, and -6.9 dB and -8.7 dB with 32 repetitions, respectively. As expected, the results in EPA1 channel outperform the results in ETU1 channel, since the latter is associated with more severe propagation conditions compared to EPA1 as outlined in [23]. Interestingly, the obtained results constitute a new reference for NPRACH detection performance in practical system configurations, since none of the existing works provides the performance analysis of the respective method in practical scenarios, but solely the performance with respect to the 3GPP requirements, i.e., with fixed CFO and single UE.

E. Complexity Analysis

In order to justify the use of the proposed method in practical scenarios, we provide also a complexity analysis and a comparison with the complexity of the mentioned state-of-the-art works. The complexity comparison with [9] is not needed since it apparently has a much higher complexity than our method due to the mentioned 2-D-FFT calculation (our method requires a single 1-D-FFT calculation). Hence, we focus on the number of complex multiplications required by the proposed method and by the method from [13].

In [13], the frequency estimation block requires a number of complex multiplications of $\approx 4N_{\text{rep}}^{\text{NPRACH}}+2$. On the other hand, the compensation block requires $4N_{\text{rep}}^{\text{NPRACH}}$ complex multiplications. For the ToA estimation part, no multiplication is required since the calculated symbols during the frequency estimation and compensation stages can be reused. Only 1-D-FFT is required in this part. However, $\approx$ 5 real multiplications ($\approx$ 1 complex multiplication) are needed to: 1) calculate the square of absolute value of the metric; 2) deduce ToA; 3) obtain quadratic interpolation factor; and 4) perform the correction of the estimated ToA using the interpolation factor. We

note that all multiplications by a factor 2^n are not considered since they can be implemented via shift registers. Taking into account the maximum UEs that can simultaneously send their NPRACH in NB-IoT (i.e., 48 UEs), the overall complexity in term of complex multiplication is about $\mathcal{O}(48 \cdot 8N_{\text{rep}}^{\text{NPRACH}})$ in addition to a 1-D-FFT with 256 points per receiver antenna.

Regarding the proposed method, the complexity estimation is done first for the minimum combination and then for the extended combinations. For the minimum combinations, the ToA estimation part requires $4N_{\text{rep}}^{\text{NPRACH}} - 1$ complex multiplications in addition to 1-D-FFT with 256 points. The same real multiplications as [13] are required (i.e., $\approx$ 5 real multiplications). For 48 UEs, the overall complexity for the minimum combination is $\mathcal{O}(48 \cdot 4N_{\text{rep}}^{\text{NPRACH}})$ in addition to a 1-D-FFT with 256 points per receiver antenna. Clearly, the proposed method with minimum combinations has 50% less complexity compared to [13]. With the extended combinations, the ToA estimation requires $8N_{\text{rep}}^{\text{NPRACH}} - 3$ in addition to the same aforementioned real multiplications and one 1-D-FFT of 256 points. In total, the complexity of the maximum combinations is $\mathcal{O}(48 \cdot 8N_{\text{rep}}^{\text{NPRACH}})$ in addition to a 1-D-FFT per receiver antenna. Obviously, even with the extended combination, the complexity of the proposed method is not higher[3] than the complexity of the algorithm proposed in [13].

This analysis proves that the proposed method has the lowest complexity compared to the state-of-the-art works. Taking into account the mentioned performance improvements, our method is in fact a very promising solution for realistic scenarios of NB-IoT.

V. Conclusion

In this article, a novel reception method for NB-IoT RA has been presented. The proposed method is designed in a way that the CFO present in the received signal is perfectly eliminated. An extended version of the method is also proposed. The method has been simulated under the 3GPP conditions to test its conformity toward 3GPP requirements. Comparisons with relevant state-of-the-art work are also provided. The obtained results and complexity analysis illustrated the effectiveness of the proposed method in term of flexibility, low-complexity and high accuracy of ToA estimation. Here, the flexibility results from the fact that the proposed method: 1) eliminates perfectly the CFO, and performs equally well with any CFO and 2) supports both preamble formats 0 and 1. Moreover, the absence of the CFO estimation and compensation reduce considerably the computational complexity leading to $\approx$ 50% complexity savings compared to the previous work. Last but not least, 8.5 to 10 dB margins are obtained under a realistic scenario (EPA1 channel) compared to 3GPP requirements. The capabilities of the proposed method can be exploited in order to reduce the length of the NPRACH preamble. Correspondingly, successful synchronization can be achieved much faster, which would allow to relax the hardware design, reduce the power consumption of the IoT UEs and contribute to the overall throughput increase of the system saving thus the scarce system resources.

[3]More precisely, our method requires four less multiplications per user per antenna than [13], which leads to $48 \cdot 4 = 192$ fewer multiplications in total.

Appendix
Assumptions on NB-IoT Propagation Channel

1) Coherence Time: The coherence time is defined as a measure of the expected time duration over which the propagation channel can be viewed as constant. Essentially, it is related to the relative motion between the transmitter and the receiver. In order to calculate the coherence time T_0, we consider the maximum Doppler frequency $F_d = 1$ Hz defined for NB-IoT in 3GPP standard, see [10]. According to the lower bound on the coherence time in [24], T_0 can be calculated via

$$T_0 = \frac{9}{16\pi F_d}. \tag{22}$$

From this, we can deduce that the coherence time T_0 is around 179 ms. Hence, the channel remains constant for a sufficient number of SGs ($\approx$ 111 SGs).

2) Coherence Bandwidth: The coherence bandwidth is defined as the frequency range with a high amplitude correlation, i.e., the frequency band with a sufficient flatness of the channel. The lower bound on the coherence bandwidth F_0 depending on the root mean-squared (rms) delay spread σ_{rms} is given by [24]

$$F_0 = \frac{1}{50\sigma_{rms}}. \tag{23}$$

In NB-IoT, the frequency hopping is used within 12 subcarriers [8]. In other words, the preamble signal is restricted within a bandwidth of 45 kHz (equivalent to 12 subcarriers). On the other hand, taking into account the delay spread of the EPA channel of $\sigma_{rms} \approx 45$ ns [23], $F_0 \approx 444$-kHz results. Hence, the channel is flat within 45 kHz.

From this analysis, we conclude that the assumptions made in Section II are correct.

References

[1] "Cellular IoT evolution for industry digitalization," Ericsson, Stockholm, Sweden, White Paper, Jan. 2019. [Online]. Available: https://www.ericsson.com/en/white-papers/cellular-iot-evolution-for-industry-digitalization

[2] "LoRaWAN, what is it?" in *A Technical Overview of LoRa© and LoRaWAN©*, LoRa-Alliance, Fremont, CA, USA, Nov. 2015. [Online]. Available: https://lora-alliance.org/resource-hub/what-lorawanr

[3] *Sigfox*. Accessed: Nov. 2015. [Online]. Available: http://www.sigfox.com

[4] *LTE; Evolved Universal Terrestrial Radio Access (E-UTRA) and Evolved Universal Terrestrial Radio Access Network (E-UTRAN); Overall Description, Version 13.2.0 Release 13*, 3GPP Standard TS 36.300, Jan. 2016.

[5] J. Schlienz and D. Raddino, "Narrowband Internet of Things whitepaper," Rohde&Schwarz, Munich, Germany, White Paper, pp. 1–42, 2016.

[6] M. Elsaadany, A. Ali, and W. Hamouda, "Cellular LTE-A technologies for the future Internet-of-Things: Physical layer features and challenges," *IEEE Commun. Surveys Tuts.*, vol. 19, no. 4, pp. 2544–2572, 4th Quart., 2017.

[7] A. Rico-Alvarino *et al.*, "An overview of 3GPP enhancements on machine to machine communications," *IEEE Commun. Mag.*, vol. 54, no. 6, pp. 14–21, Jun. 2016.

[8] *LTE; Evolved Universal Terrestrial Radio Access (E-UTRA); Physical Channels and Modulation, Version 13.7.1 Release 13*, 3GPP Standard TS 36.211, Oct. 2017.

[9] X. Lin, A. Adhikary, and Y.-P. Wang, "Random access preamble design and detection for 3GPP narrowband IoT systems," *IEEE Wireless Commun. Lett.*, vol. 5, no. 6, pp. 640–643, Dec. 2016.

[10] *LTE; Evolved Universal Terrestrial Radio Access (E-UTRA); Base Station (BS) Radio Transmission and Reception, Version 14.3.0 Release 14*, 3GPP Standard TS 36.104, Apr. 2017.

[11] X. Lin, Y.-P. Wang, and A. Adhikary, "Preamble detection and time-of-arrival estimation for a single-tone frequency hopping random access preamble," U.S. Patent US20 170 324 587 A1, Nov. 2017.
[12] J. Hwang, C. Li, and C. Ma, "Efficient detection and synchronization of superimposed NB-IoT NPRACH preambles," *IEEE Internet Things J.*, vol. 6, no. 1, pp. 1173–1182, Feb. 2019.
[13] A. Chakrapani, "NB-IoT uplink receiver design and performance study," *IEEE Internet Things J.*, vol. 7, no. 3, pp. 2469–2482, Mar. 2020.
[14] *NPRACH Demodulation Requirements*, document R4-168206, 3GPP TSG-RAN WG4 Meeting #80bis, Ericsson, Stockholm, Sweden, Oct. 2016.
[15] *LTE; Evolved Universal Terrestrial Radio Access (E-UTRA); Radio Resource Control (RRC); Protocol Specification, Version 13.8.1 Release 13*, 3GPP Standard TS 36.331, Jan. 2018.
[16] *Narrowband LTE—Random Access Design*, document R1-156011, 3GPP TSG-RAN1 #82bis, Ericsson, Stockholm, Sweden, Oct. 2015.
[17] *NB-IoT—Random Access Design*, document R1-157424, 3GPP TSG-RAN1 #83, Ericsson, Stockholm, Sweden, Nov. 2015.
[18] *NB-IoT—Design considerations for single tone frequency hopped NB-PRACH*, document R1-160093, 3GPP TSG-RAN1 AH-NB-IoT, Ericsson, Stockholm, Sweden, Jan. 2016.
[19] *NB-IoT—Single Tone Frequency Hopping NB-PRACH Design*, document R1-160275, 3GPP TSG-RAN1 #84, Ericsson, Stockholm, Sweden, Feb. 2016.
[20] "Technical specification group GSM/EDGE radio access network; cellular system support for ultra low complexity and low throughput Internet of Things; (release 13), v2.1.0," 3GPP, Sophia Antipolis, France, 3GPP Rep. TR 45.820, Aug. 2015.
[21] D. Rife and R. Boorstyn, "Single tone parameter estimation from discrete-time observations," *IEEE Trans. Inf. Theory*, vol. 20, no. 5, pp. 591–598, Sep. 1974.
[22] M. Abe and J. O. Smith, *Design Criteria for Simple Sinusoidal Parameter Estimation Based on Quadratic Interpolation of FFT Magnitude Peaks*, Audio Eng. Soc. Convention, San Francisco, CA, USA, 2004.
[23] *3rd Generation Partnership Project; Technical Specification Group Radio Access Network; Evolved Universal Terrestrial Radio Access (E-UTRA); User Equipment (UE) Radio Transmission and Reception; (Release 8), Version 1.1.0*, 3GPP Standard TS 36.803, Apr. 2008.
[24] B. Sklar, "Rayleigh fading channels in mobile digital communication systems .I. Characterization," *IEEE Commun. Mag.*, vol. 35, no. 7, pp. 90–100, Jul. 1997.

Houcine Chougrani received the State Engineering degree in electronics from Ecole Nationale Polytechnique Algiers, El Harrach, Algeria, in 2011, the M.S. degree in signal processing from Paul Sabatier University, Toulouse, France, in 2012, and the Ph.D. degree in information technology from Ecole Telecom Bretagne, Brest, France, in 2016.

From 2017 to 2018, he was an R&D Engineer with the Department of Telecommunication, Airbus Defence and Space, Toulouse, France, where he worked on the design of communication protocols for satellite payloads both on the system and physical layer levels. From 2018 to 2019, he was an R&D Engineer with OQ Technology, Luxembourg City, Luxembourg, where he worked on the integration of IoT protocol for satellite communication. He is currently a Research Associate with the Interdisciplinary Centre for Security, Reliability and Trust, University of Luxembourg, Luxembourg City. His research interests include wireless communication theory, satellite communication and new radio for the Internet-of-Things applications.

Steven Kisseleff (Member, IEEE) received the M.Sc. degree in information technology from the Technical University of Kaiserslautern, Kaiserslautern, Germany, in 2011, and the Ph.D. degree in electrical engineering from the Friedrich-Alexander University of Erlangen–Nürnberg (FAU), Erlangen, Germany, in 2017.

He was a Research and Teaching Assistant with the Institute for Digital Communications, FAU, from October 2011 to July 2018. From 2012 to 2013, he was a Visiting Researcher with the State University of New York, Buffalo, NY, USA, and the Broadband Wireless Networking Lab, Georgia Institute of Technology, Atlanta, GA, USA. In 2018, he joined the Interdisciplinary Centre for Security, Reliability and Trust, University of Luxembourg, Luxembourg City, Luxembourg, as a Research Associate. His research activities are mainly focused on the satellite communications, random access, and reconfigurable intelligent surfaces.

Symeon Chatzinotas (Senior Member, IEEE) received the M.Eng. degree in telecommunications from the Aristotle University of Thessaloniki, Thessaloniki, Greece, in 2003, and the M.Sc. and Ph.D. degrees in electronic engineering from the University of Surrey, Guildford, U.K., in 2006 and 2009, respectively.

He is currently a Full Professor/Chief Scientist I and the Co-Head of the SIGCOM Research Group at SnT, University of Luxembourg, Luxembourg City, Luxembourg. In the past, he has been a Visiting Professor with the University of Parma, Parma, Italy. He was involved in numerous Research and Development projects for the National Center for Scientific Research Demokritos, the Center of Research and Technology Hellas, and the Center of Communication Systems Research, University of Surrey. He has coauthored more than 400 technical papers in refereed international journals, conferences and scientific books.

Prof. Chatzinotas was a co-recipient of the 2014 IEEE Distinguished Contributions to Satellite Communications Award, the CROWNCOM 2015 Best Paper Award, and the 2018 EURASIC JWCN Best Paper Award. He is currently on the Editorial Board of the IEEE OPEN JOURNAL OF VEHICULAR TECHNOLOGY and the *International Journal of Satellite Communications and Networking*.